



An investigation on the corrosion behaviour of B₄C-reinforced AA5083 aluminium alloy in sodium chloride solution using electrochemical impedance spectroscopy

KOUROSH JAFARZADEH*, HAMED ANSARI ASHLAGHI, ALI ALIZADEH
and HADISEH MAZHARI ABBASI 

Faculty of Materials and Manufacturing Technologies, Malek Ashtar University of Technology, Tehran 15875-1774, Iran

*Author for correspondence (kjafarzadeh@mut.ac.ir)

MS received 3 December 2023; accepted 18 March 2024

Abstract. In this research, the role of B₄C-reinforcing particles on the corrosion behaviour of Al5083/B₄C nanocomposite has been investigated. Al/B₄C nanocomposite powder with weight percentages of 3 and 7 of reinforcing phase was prepared by mechanical milling method. The resulting powder was initially hot-pressed and then hot-extruded. The microstructure of the sample was studied using scanning electron microscopy and their corrosion behaviour was studied using potentiodynamic polarization and scanning electrochemical impedance spectroscopy methods in different immersion time intervals. The results showed a uniform distribution of reinforcing particles and also the scattering of intermetallic particles at the surface of the samples. However, increasing the content of B₄C particles in the composite samples enhances the cathodic and anodic reactions by increasing the content of intermetallic particles as cathodic sites on the surface, so that higher corrosion current density is observed in the composite samples with 7 wt% B₄C. Finally, it was concluded that increasing the value of B₄C decreases the corrosion resistance of the B₄C-reinforced composite samples in sodium chloride solution, which makes it unsuitable in marine applications.

Keywords. AA5083 aluminium alloy; composite; B₄C; corrosion; sodium chloride solution.

1. Introduction

Aluminium matrix composites are produced by dispersing hard particles such as oxides, carbides, nitrides and borides in the aluminium substrate. These materials are used in the aerospace and automotive industry because of their low density, high strength, good abrasion resistance, high-temperature properties and high modulus [1–4]. Although the presence of the second phase as the metal reinforcement increases the physical and mechanical properties of the material, it can change its corrosion behaviour. In the presence of reinforcing particles, it is possible that the corrosion resistance of the materials increases or decreases [5,6].

The corrosion behaviour of alloys depends on the electrochemical potential of intermetallic particles which are usually electrically conductive. So some particles have a more negative potential than the matrix, some have the same potential and some have a more positive potential than the matrix. While the potential of reinforcement is more positive than that of the aluminium matrix, it results in the galvanic corrosion of the aluminium alloy and forms pitting. There is no galvanic corrosion when the reinforcements are equipotential with the matrix. In the alloys in which the

potential of conductive reinforcement is more negative than the matrix, the particle is dissolved first and the matrix is cathodically protected [7–9].

In all above-mentioned researches, only the role of intermetallic particles in the corrosion behaviour of aluminium alloy has been investigated. These particles have a different nature from ceramic particles, which are nonconductive. Therefore, it is essential to study the corrosion behaviour of aluminium composites in the presence of ceramic particles.

Studying the corrosion behaviour of Al2024/Al₂O₃ composite by Karabulut and Karacif [10] showed that with increasing Al₂O₃, corrosion resistance of the composite increases higher content of Al₂O₃ as a nonconductive corrosion-resistant compound [10]. However, another mechanism was experienced in the research by Abbass and colleagues [11]. They observed that the corrosion rate of 6061Al containing various percentages of SiC, increases due to galvanic corrosion between the reinforcement and the matrix [11]. In studying the Al6061/SiC composite, Ahmed [12] concluded that increasing the volume fraction of the second phase leads to increased corrosion rate by increasing the cathodic areas. On the other hand, it has been determined that the SiC particles can affect the corrosion

behaviour of the aluminium metal–matrix composite, by changing and increasing the distribution of the intermetallic phase in the aluminium alloy, which finally increases the corrosion rate [12]. One of other researchers [13] also showed that the corrosion behaviour of Al2024/SiC composites can be modified by decreasing the size of the reinforcing particles. The appearance of an inductive loop in EIS plot of an SiC-reinforced aluminium composite in sodium chloride solution has proved the hypothesis of the authors that pitting corrosion in this composite has resulted in the presence of chloride ions in the solution.

Although it was observed in all the above cases that the presence of secondary phase particles has a negative effect on the corrosion behaviour of composites, as mentioned in the previous sections, these particles show different electrochemical behaviours. In addition, previous researches by the authors [14] have shown that oxygen is the key factor in pitting corrosion of aluminium alloys, and these alloys are corroded and localized even in distilled water. Therefore, it is necessary to study and investigate the corrosion behaviour of each composite material in the presence of particles with different percentages.

Al–B₄C is one of the composites that have been introduced in recent years to the industry. Its lower density and comparable mechanical and thermal properties to SiC and aluminium make it a proper selection for applications such as neutron absorption, wear and impact resistance [15].

Majority of research on Al/B₄C composites has concentrated on their mechanical and physical characteristics, such as their high surface hardness [16], wear resistance [17] and tensile strength [4,18–20]. Most researchers have concluded that the mechanical properties of the composites can be improved, at least to some extent, by increasing the fraction and decreasing the size of B₄C. On the other hand, not much is known about this material's corrosion behaviour. Due to the increasing use of this material in various industries, the need for research in this field has increased.

It is known that the aluminium AA5083 alloy with magnesium content of about 4–5 wt% has properties such as low density, high strength and high corrosion resistance, and consequently is utilized in marine industries, including submarine and radar boats [21–23]. It is predicted that by reinforcement of this matrix with B₄C, it converts to a composite with special physical and mechanical properties due to the fact that this reinforcement is one of the hardest and lightest ceramics [19,20], consequently, these materials can be used in the construction of marine structures provided to obtaining high corrosion resistance in these composites in sodium chloride solution. Vasudevan *et al* [24] used the stir casting method to create an alloy called AA5083 that was composited with B₄C at a content of more than 7 wt% in one of their research projects. Nonetheless, they assessed the alloy's resistance to corrosion using the salt spray method. They came to the conclusion that an increase in B₄C particle content reduces the composite's resistance to corrosion [24]. In a different study,

Katkar *et al* [25] looked into how B₄C reinforcement affected the corrosion of AA6061 alloy that was composited with B₄C at weight percentages greater than 10%. When comparing the composite to the base alloy, they saw a positive shift in its potential. Furthermore, the addition of B₄C causes the composite's corrosion rate to increase significantly [25]. Despite the aforementioned studies, it appears that the composite's corrosion behaviour is improved by alterations in the composite's fabrication process and the addition of B₄C particles. Therefore, the purpose of this study was to investigate the effect of reinforcement of boron carbide on the corrosion behaviour of Al5053/B₄C composite produced by mechanical alloying and extrusion in sodium chloride solution and its comparing with the corrosion behaviour of AA5083 aluminium alloy. Electrochemical impedance spectroscopy was utilized as a nondestructive method to analyse the behaviour more.

2. Experimental

In this research, AA5083 aluminium powder with an average size of 45 µm as a matrix and boron carbide powder with an average size of 20 µm as a reinforcement phase were used to fabricate the composite. Al/B₄C powders containing 3 and 7 wt% of reinforcing phases were ground by a high-energy planetary mill in an argon atmosphere with a purity of 99.999% for 50 h. After the mechanical alloying process, the hot pressing method was used to compress and produce the first powdered moulds. For this purpose, the powder was first compressed by hydraulic press with a capacity of 60 tons, in a cylindrical matrix with a diameter of 3 cm, with a socket for 15 min. In order to achieve the necessary compression and porosity removal, the compressed samples were placed at 550°C under a hot extrusion process to produce composite rods of 1 cm diameter. Extruded samples were first cut in transverse direction and the surface preparation of the samples was carried out up to the grit of 1200 with abrasive paper. The sample was then etched with an etchant with the composition and conditions are presented in table 1.

AA5083-H321 aluminium alloy was also used for comparison and studying the effect of boron carbide on the properties of AA5083 aluminium alloy.

All the samples were immersed in sodium chloride solution, and their electrochemical behaviour was investigated at time intervals of 1, 5, 24, 72 and 240 h.

Table 1. Composition of etchant for microscopic studies of the samples

HF	Distilled water	Temperature	Time
0.5 ml	99.5 ml	25°C	5 min

The microstructure of the samples before and after the removal of corrosion products was studied by Tescan vega3 scanning electron microscope model 8040SU to determine how the secondary phase was distributed in the metal. Removal of corrosion products from the surface was done by a solution of 50 ml phosphoric acid, 20 g chromic acid at a temperature of 90°C for 10 min [14].

Potentiodynamic polarization tests were done by a Potentionstat/Galvanostat Biologic-VSP 300 in the range of 250 to 1000 mV vs. saturated calomel electrode (SCE), with a scan rate of 0.2 mV s⁻¹ in 3.5 wt% NaCl solution. The same instrument and the electrolyte was utilized for EIS tests with a frequency range of 100 KHz to 10 mHz, with potential amplitude of ±10 mV while the samples were in their open-circuit potential. In all the electrochemical tests, platinum was considered as counter electrode.

The data were then analysed using Zview2 and EC-Lab software. Effective capacitance was calculated for all the time constants in accordance with equation (1) [26,27].

$$C = T^{\frac{1}{n}} \left(\frac{1}{R_{ct}} + \frac{1}{R_f} \right)^{\frac{n-1}{n}} \quad (1)$$

In which C is effective capacitance (F cm⁻²), R_f is film resistance (ohm cm²), R_{ct} is charge transfer resistance (ohm cm²), T is admittance (F cm⁻² sⁿ⁻¹) and n is a number between 0 and 1.

3. Result and discussion

3.1 SEM analysis

Figure 1 shows the scanning electron microscopy (SEM) images from the surface of AA5083 aluminium alloy, and the composites with 3 and 7 wt% B₄C, before immersion in sodium chloride solution. As can be seen in this figure, the size of the reinforcements in the composite samples is about 100 nm, which is much smaller than the intermetallic particles in AA5083 aluminium alloy. In addition, the elemental analysis from the surface of composite samples indicates that the amount of intermetallic particles in these composites has also increased compared to AA5083 aluminium alloy sample. An analysis taken from the surface of composite samples suggests that dark particles in the image are particles of B₄C and the amount of alloying elements around the particles is greater than the matrix [14,28].

In accordance with the previous researches, application of shear stresses during the extrusion and mechanical milling operations [28], results in the crushing of intermetallic particles and their widespread distribution within the composite. This increases the contact surface area of these cathodic particles with sodium chloride solution. On the other hand, during the mechanical milling operation, the increase of impurities such as iron, silicon and manganese in the sample results in an increase in the percentage of the

intermetallic particles that leads to the expansion of the sites with different potentials compared to the uncomposited samples. In composite operations by adding the reinforcing particles, the difference in the thermal expansion coefficients and the elastic modulus between the matrix and the particles, leads the dislocation density increases in the matrix of the composite. Migration of dislocations itself applies shear stresses to the brittle intermetallic particles, which consequently makes them finer [29].

Figure 2 shows the samples of AA5083 aluminium alloy and the composite samples with 3 and 7 wt% B₄C after 24 h immersion in sodium chloride solution. It is observed that the corrosion in the composite samples is much more severe than AA5083 aluminium alloy.

As can be seen in figure 2a, pitting corrosion has occurred in the vicinity of intermetallic particles in AA5083 aluminium alloy. In fact, around these cathodic intermetallic particles are preferred locations for pitting corrosion. The EDS analysis of these intermetallic particles in this figure indicates that they contain iron, copper, chromium, manganese, silicon, and magnesium.

The pitting corrosion mechanism of AA5083 aluminium alloy has been explained in detail by the previous studies [14,21]. However, in composite samples, a cracked morphology is observed on the surface. In addition, intermetallic particles containing the elements such as Fe, Cr and Al are also detectable in the composite samples. These elements give the cathodic behaviour to the intermetallic particles. Cathodic behaviour of the intermetallic particles tends pitting corrosion on the surface of the composite samples. SEM results in figure 2c and d emphasize to this. It is seen that pits have been appeared on the surface of the samples after removing of the corrosion products.

3.2 Polarization plots

Figure 3 shows the potentiodynamic polarization plots of different samples in a solution of 3.5 wt% sodium chloride. Table 2 also indicates the data obtained from these plots.

As can be seen in the plots of figure 3, a passive behaviour is observed in the polarization plot of AA5083 aluminium alloy. However, the plots of the composite samples do not show any passivity in the anodic branch. The data in table 2 also indicates that, addition of reinforcement particles to the aluminium matrix makes its corrosion potential more negative, which indicates the higher potential of the composite samples for corrosion in sodium chloride solution. Corrosion current density in the composite sample also increased by 15 and 18 times compared to AA5083 aluminium alloy, which indicates the high corrosion rate of these composites in sodium chloride solution. According to SEM images of the samples in figure 2, except in AA5083 aluminium alloy, in other samples, the distribution of intermetallic particles in the matrix and occurrence of oxygen reduction as cathodic reaction and the formation

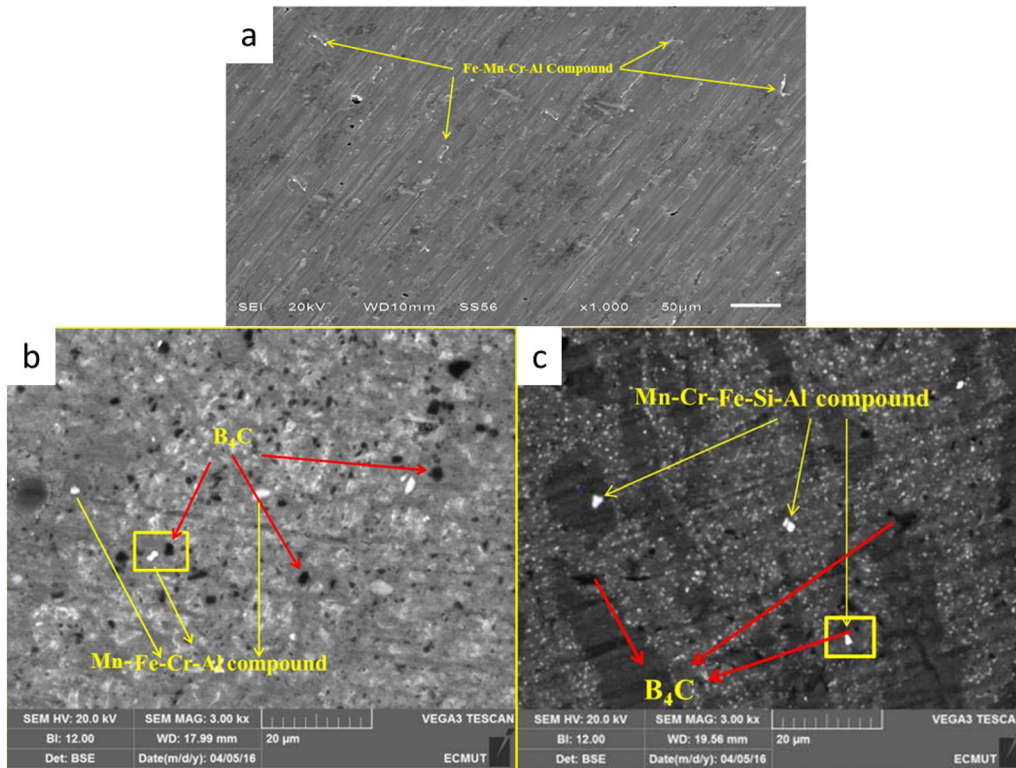


Figure 1. Scanning electron microscopy image of the surface of (a) AA5083 aluminium alloy, (b) Al-3 wt% B₄C and (c) Al-7 wt% B₄C before immersion in sodium chloride solution.

of alkaline medium at the whole surface of the sample [14], the passive layer on the sample is dissolved, which results in an increase in the corrosion rate of these samples compared to AA5083 aluminium alloy.

In composite samples, due to the scattering of intermetallic particles or the expansion of cathodic sites, both the cathodic and anodic reactions are intensified that eventually results in adsorption of chloride ions in the solution. This increases the amount of chloride ions on the surface, which consequents the formation of a layer of chlorine-rich product. Considering the high concentration of chlorine and the high percentage of aluminium in EDS analysis of figure 4, it can be said that after immersion of the samples in a sodium chloride solution, the layer of $\text{Al}(\text{OH})_2\text{Cl}_2^-$, which is soluble in sodium chloride solution, is formed on the surface of the sample [13]. Figure 2d and e shows a cracked morphology of this layer. These cracks can be due to the thickening and tensile stresses in the $\text{Al}(\text{OH})_2\text{Cl}_2^-$ layer, which enhances the dissolution of this layer in sodium chloride solution. By comparing figure 2a with b and c, it seems that, unlike AA5083 aluminium alloy, no passive layer is formed on the surface of composite samples. It is observed that in Al-7 wt% B₄C, with increasing the percentage of reinforced particles, the degradation caused by corrosion in this sample is much more severe than the other samples, so that the layer of

$\text{Al}(\text{OH})_2\text{Cl}_2^-$ which is completely discontinuous is seen as islands on the surface. This indicates the intense dissolution of this layer after immersion of the sample in a sodium chloride solution.

3.3 EIS results

Figure 5 shows the Nyquist plots of the electrochemical impedance spectroscopy studies of the AA 5083 aluminium samples. The plot shows two capacitive time constants in the high and low frequencies at all the immersion times. So, the diameters of the capacitance arcs decrease with an increase in immersion time. As mentioned in the introduction, the existence of intermetallic particles with a cathodic nature is the cause of the pitting corrosion in these alloys. In fact, the different chemical composition of the intermetallic particles and the matrix creates a galvanic cell between these two components. The cathodic reaction in this cell is the reduction of oxygen and the formation of hydroxyl ion (equation (2)), which results in the dissolution of the oxide layer surrounding the intermetallic particles. The corresponding anodic reaction is the development of a passive layer on the matrix and an increase in the thickness of this layer (equation (3)). In addition, the reaction of aluminium with chloride ions in

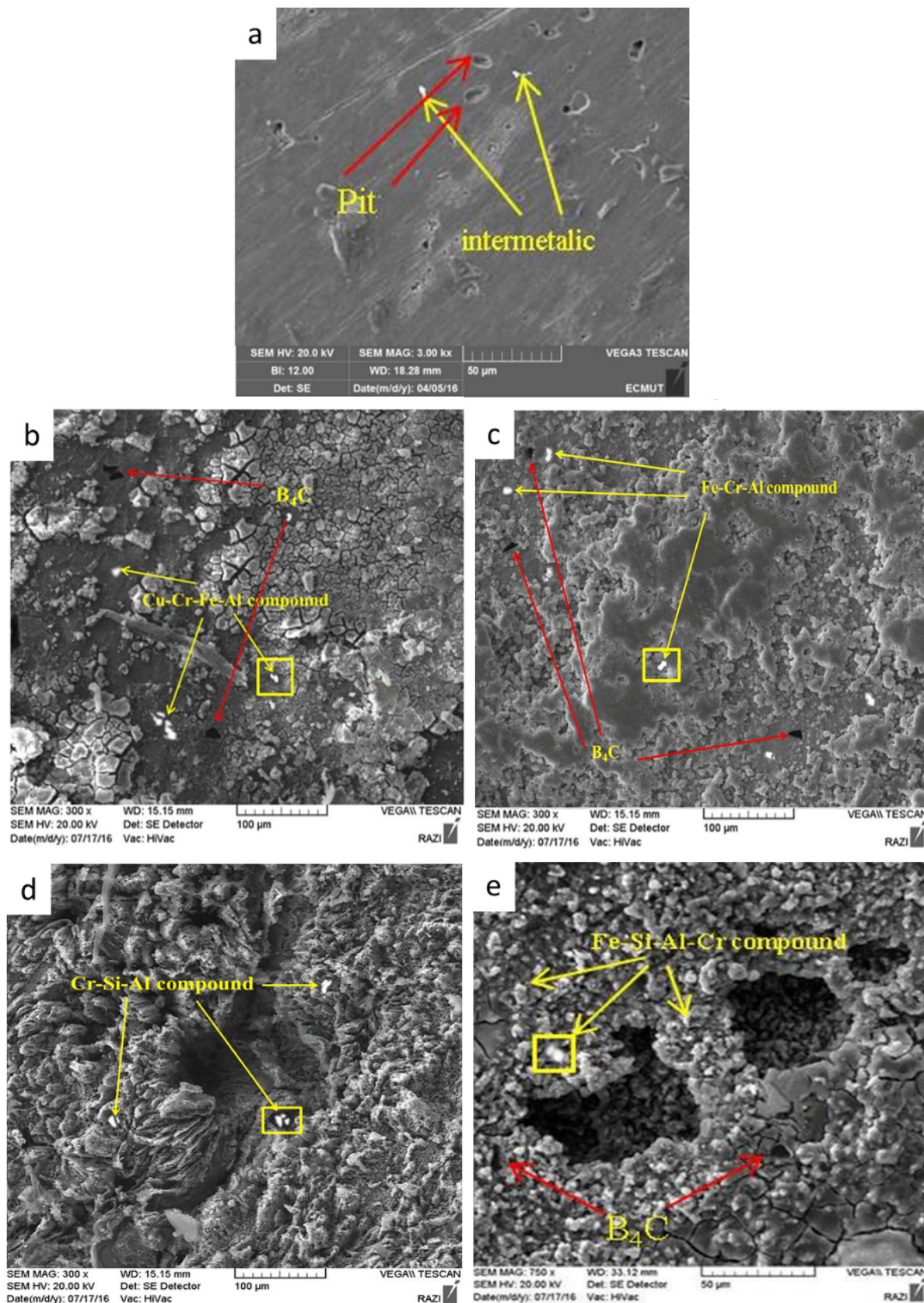


Figure 2. Scanning electron microscopic images of the surface of (a) AA5083 aluminium alloy after removal of the corrosion product, (b) Al-3 wt% B₄C and (c) Al-7 wt% B₄C, after 24 h immersion and before removal of corrosion product, (d) Al-3 wt% B₄C and (e) Al-7 wt% B₄C after removal of the corrosion product.

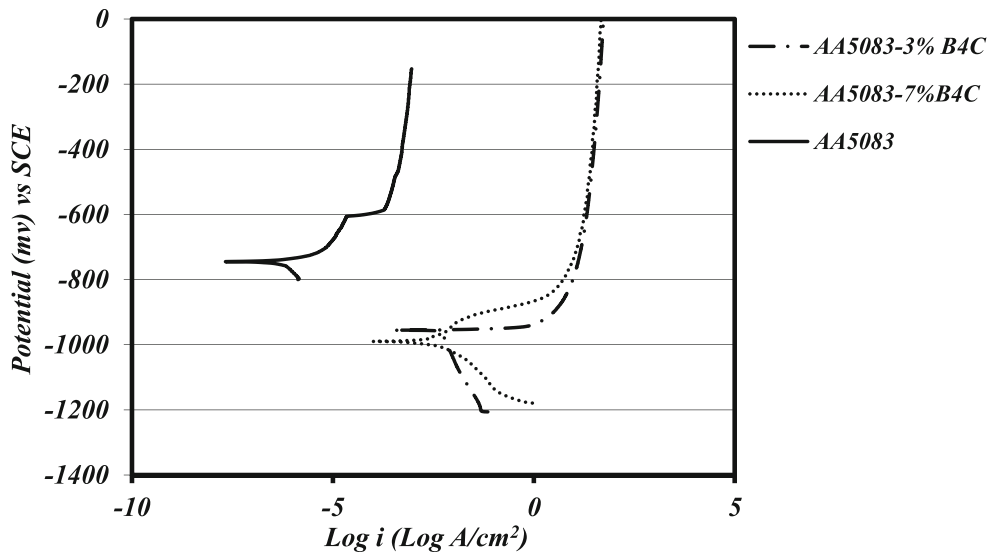
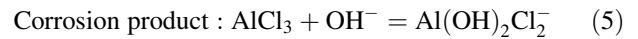
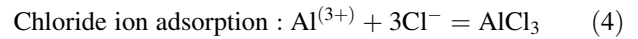
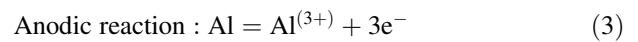
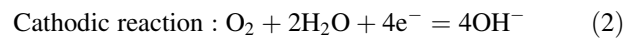


Figure 3. Potentiodynamic polarization plots of the samples in 3.5 wt% sodium chloride solution.

Table 2. Data obtained from the analysis of the plots in figure 3.

Sample	E_{corr} (mV _{SCE})	i_{corr} ($\mu\text{A cm}^{-2}$)
AA5083 aluminium alloy	-770	3.54
Al5083-3 wt% B ₄ C	-1050	65
Al5083-7 wt% B ₄ C	-1120	55

the solution can cause corrosion around the intermetallic particles (equations 4-5)



Therefore, considering these cases and taking into account the position of the components in relation to each other in the alloy in figure 6, the circuit of figure 7 containing two time constants is presented for fitting of the impedance data, in which R_s is the uncompensated resistance between the working and reference electrodes; R_f is the resistance of existing layers on the surface and the passive layer on the intermetallic particles; T_f is the constant phase element of the layers on the surface and the passive layer on intermetallic particles; T_{dl} is the constant phase element of the electrical double layer on the surface and the passive layer on the intermetallic particles and R_{ct} is the charge transfer resistance.

Figure 5 shows that the data obtained from the equivalent circuit are in good agreement with the experimental data of the impedance test taken from the sample after 1 h immersion in the solution. Due to the fact that the mechanism of reactions on the surface does not change with increasing immersion time, so at immersion times of more than 1 h, all the data obtained with the circuit of figure 7 can be justified.

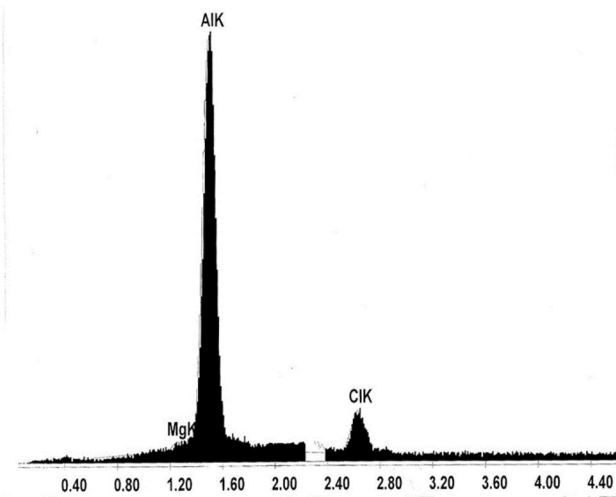


Figure 4. EDS analysis from the surface of corrosion product on the surface of composite samples.

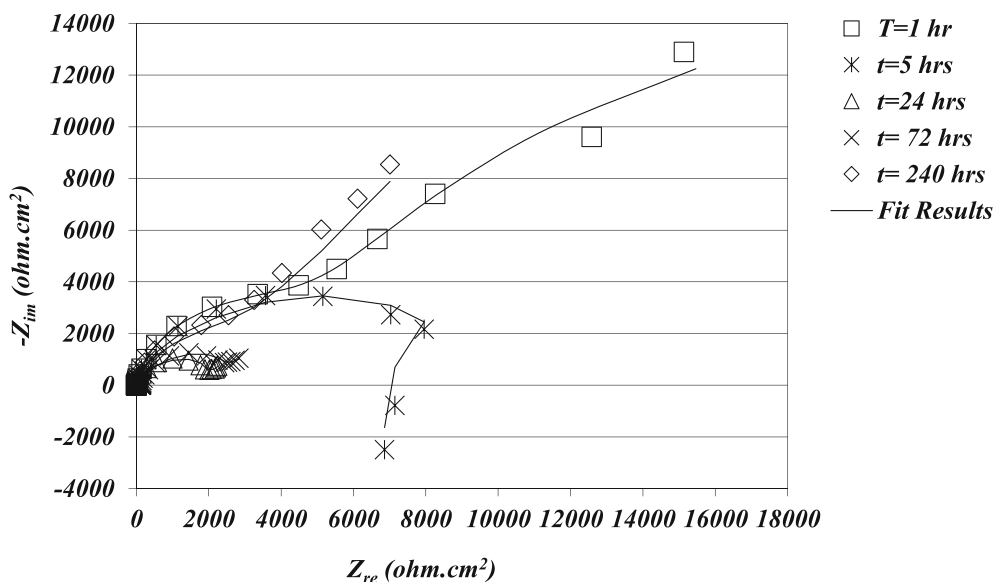


Figure 5. Nyquist plots of the electrochemical impedance spectroscopy studies of the AA5083 aluminium samples at different immersion times to sodium chloride solution.

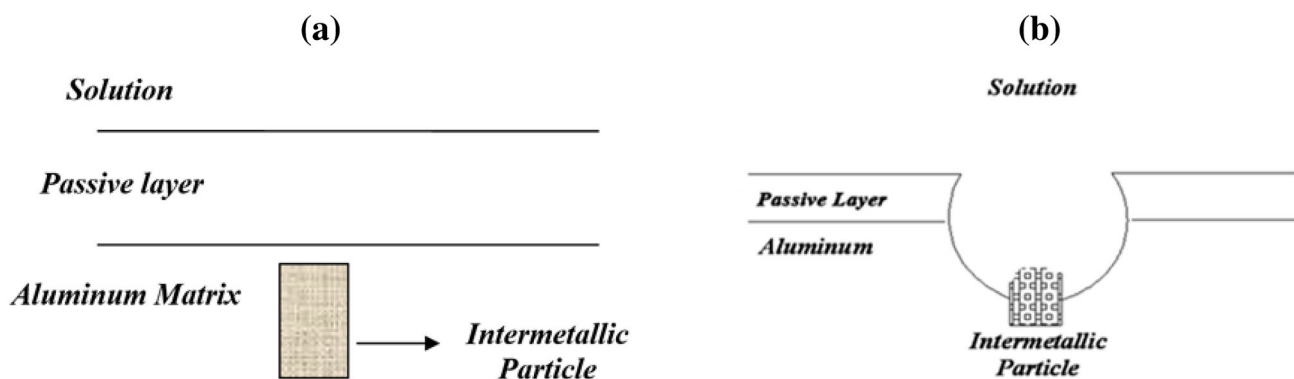


Figure 6. Cross-sectional schematic of AA5083 aluminium alloy and position of intermetallic particles in the alloy (a) before and (b) after pitting corrosion in sodium chloride solution.

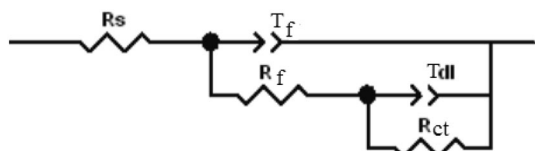


Figure 7. Electrical equivalent circuit for the fitting of impedance data taken from AA5083 aluminium alloy.

The electrical parameters obtained by fitting the experimental data to the electrical equivalent circuit proposed in figure 7 are shown in table 3.

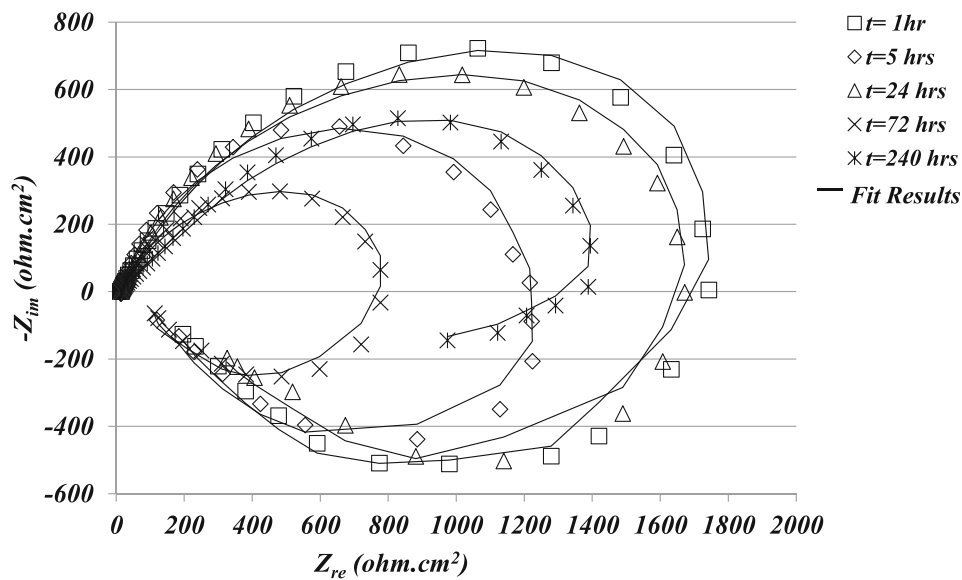
It was observed in the polarization plots in figure 3 that, there is still a passive layer on the surface of AA5083 aluminium alloy at 1 h immersion of the sample in the solution. The presence of the passive layer on the surface tends a high value of R_f and n_f , which give a higher value of $C_{eff(f)}$. However, inhomogeneous cathodic

and anodic reactions on the surface is seen into the low value of n_{dl} in the EIS data in table 3 at the beginning of the immersion time. This inhomogeneity in the cathodic and anodic reactions that were explained previously by equation (2) up to equation (5) tends to pit corrosion initiates on the surface, which is seen in the decreasing of R_{ct} by extension of immersion time. Fluctuation of n_f , R_f , $C_{eff(f)}$, n_{dl} , R_{ct} and $C_{eff(dl)}$ indicate periodic accumulation of corrosion products on the surface of the sample and its dissolution in the electrolyte until the end of the immersion time.

Figures 8 and 9 show the Nyquist plots for 3 and 7 wt% B_4C composite samples after different immersion times in sodium chloride solution, respectively. It is seen that the Nyquist plots of the composite samples show one capacitive and one inductive time constant in high and low frequencies, respectively. To investigate more about the origin of this form of EIS plots, the microstructure of the samples

Table 3. Data obtained from the fitting of experimental plots with the electrical equivalent circuit in figure 7 for AA5083 aluminium alloy at different immersion times in sodium chloride solution.

Time (h)	1	5	24	72	240
R_s	11.04	10.57	11.62	12.18	10.93
T_f ($F\text{ cm}^{-2}\text{ s}^{(n-1)}$)	0.000078	0.00091	0.00098	0.00056	0.000016
n_f	0.96	0.87	0.91	0.94	0.90
R_f (ohm cm^2)	2179	1067	1328	1754	1165
$C_{\text{eff}(f)}$ ($F\text{ cm}^{-2}$)	0.000072	0.00090	0.0010	0.00056	0.00001
T_{dl} ($F\text{ cm}^{-2}\text{ s}^{(n-1)}$)	0.0012	0.0140	0.0201	0.0360	0.0042
n_{dl}	0.81	0.89	0.91	0.90	0.85
R_{ct} (ohm cm^2)	5843	2371	671	1238	2798
$C_{\text{eff}(dl)}$ ($F\text{ cm}^{-2}$)	0.0019	0.0216	0.0260	0.0549	0.0065

**Figure 8.** Nyquist plots for a 3 wt% B₄C composite sample at different immersion times in sodium chloride solution.

should be investigated. Figure 10a shows the position of the intermetallic particles in a schematic way inside the composite samples before immersion in sodium chloride solution. As seen in the SEM images of figure 1, in the manufacturing process of this sample, during hot extrusion and mechanical milling, shear stresses result from grain deformation and difference in thermal expansion coefficients between the matrix and the intermetallic particles [23,29]. The shear stresses make the particles finer. The addition of fine particles and the fragmentation of the particles in the milling operation lead to the scattering and dispersion of the intermetallic particles at the sample surface [8]. In other words, the surface area of the cathodic particles exposed to sodium chloride solution increases. Based on the EDS analysis taken from these intermetallic particles indicates the presence of iron, manganese and chromium elements, which are much more cathodic

compared to aluminium in the matrix [30]. According to the above description and the electrochemical reactions which occur on the sample (equations (3) and (4)), two factors are involved in the corrosion mechanism of this alloy; the substrate and the interface of substrate and $\text{Al}(\text{OH})_2\text{Cl}_2$ corrosion product. Therefore, considering the position of the above components in the composite samples, the electrical equivalent circuit of figure 10b is presented for fitting the impedance plots for the composite samples, where R_s is the uncompensated resistance between working and reference electrodes; R_{ct} is the charge transfer resistance at the interface of substrate and the solution; T_{dl} is the constant phase element at the interface of substrate and the solution; L is the inductance resulted from adsorption of chloride ion on the surface; and R_L is the resistance of inductance resulting from the adsorption of chloride ions on the surface.

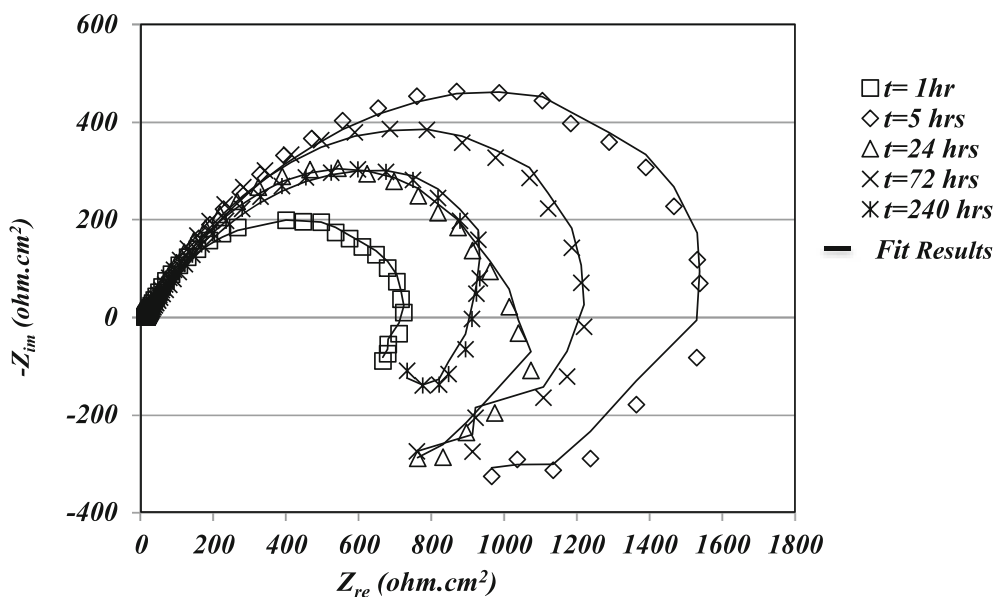


Figure 9. Nyquist plots for a 7 wt% B₄C composite sample at different immersion times in sodium chloride solution.

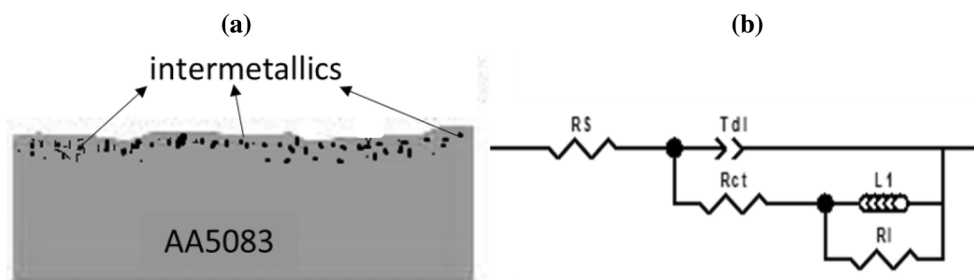


Figure 10. (a) Position of the intermetallic particles on the surface of the composite samples at high immersion time extensions. (b) The electrical equivalent circuit for fitting of EIS plots at high immersion times.

Figures 8 and 9 show that there is a good agreement between experimental data and the proposed model in figure 10 in all the immersion times. This agreement indicates that the reaction mechanism on the surface does not change with the extension of immersion time.

Potentiodynamic polarization plots in figure 3 shows that there is no passive layer on the surface of the composite samples even at the initial times of immersion. Therefore, it can be concluded that the intermetallic particles are distributed evenly on the surface, which encourages a homogeneous occurrence of cathodic reaction over the passive layer on the surface and on the intermetallic particles. With spreading of cathodic reactions on the surface, the anodic reaction which is aluminium oxidation (equation (3)), spreads on the surface in the same way. Therefore, many aluminium ions are created on the surface of the sample. The formation of Al⁺³ ions leads to the adsorption of chloride ions on the surface.

These reactions result in the formation of Al(OH)₂Cl₂⁻ layer, which is soluble in sodium chloride solution. On the other hand, in accordance with refs [31–34], it is observed that the layer formed on the surface is not continuous, and cracks are seen on it. These cracks can be caused by the local dissolution of this layer in sodium chloride solution. Finally, it is not possible to observe any passive layer on the surface.

Tables 4 and 5 present the electrical parameters obtained by fitting the experimental data to the electrical equivalent circuit proposed in figure 10b.

Comparing the EIS data in tables 4 and 5 indicates that the average value of *n_{dl}* is lower in the composite sample with 7 wt% B₄C. This means that the surface inhomogeneity is greater in this sample. In other word, this sample has shown less corrosion resistance than the sample with 3 wt% B₄C. Accumulation of Al(OH)₂Cl₂⁻ corrosion product on the surface limits the solution to reach the substrate.

Table 4. Data obtained from the fitting of experimental plots with the electrical equivalent circuit in figure 10b for 3 wt% B₄C composite sample at different immersion times in sodium chloride solution.

Time	1	5	24	72	240
R_s (ohm cm ²)	12.92	13.69	10.29	9.56	13.87
T_{dl} (F cm ⁻² s ⁽ⁿ⁻¹⁾)	0.00010	0.00016	0.00038	0.00050	0.00057
n_{dl}	0.88	0.73	0.68	0.65	0.58
R_{ct} (ohm cm ²)	575	167	159	523	345
$C_{eff(dl)}$ (F cm ⁻²)	0.00006	0.00004	0.00010	0.00024	0.00017
L (H cm ⁻²)	2846	8756	3845	2664	2267
R_L (ohm cm ²)	1104	1082	1094	1332	1119

Table 5. Data obtained from the fitting of experimental plots with the electrical equivalent circuit in figure 10b for 7 wt% B₄C composite sample at different immersion times in sodium chloride solution.

Time (h)	1	5	24	72	240
R_s (ohm cm ²)	11.27	16.94	14.90	16.77	17.65
T_{dl} (F cm ⁻² s ⁽ⁿ⁻¹⁾)	0.0004	0.00021	0.00029	0.00032	0.00040
n_{dl}	0.65	0.60	0.67	0.63	0.58
R_{ct} (ohm cm ²)	503	845	408	666	547
$C_{eff(dl)}$ (F cm ⁻²)	0.00017	0.00006	0.00010	0.00013	0.00013
L (H cm ⁻²)	9521	5428	9363	5172	9466
R_L (ohm cm ²)	245	913	661	748	393

Consequently, higher R_{ct} values are observed for the sample with 7 wt% B₄C. $C_{eff(dl)}$ but does not differ so much between the two samples. This means the active surface area in both samples is nearly the same. However, in accordance with equations (6 and 7), higher value of L and lower value of R_L in the sample with 7 wt% B₄C indicates that a higher area of the intermetallic particles in the composite samples with 7 wt% B₄C is incorporated in a cathodic reaction, which subsequently enhances the anodic reaction. In other words, the higher content of B₄C which tends to have a higher percentage of intermetallic particles intensifies the reaction of aluminium with chloride ions (equation (7)).

$$R_L = \rho \frac{L}{A}, \quad (6)$$

In which R_L is ohmic resistance of coil (ohm cm²), ρ is resistivity (ohm cm²), L the coil length (cm) and A is coil cross-surface area (cm²).

$$L = \mu_0 \mu_T N^2 \frac{A}{l}, \quad (7)$$

in which L is inductance (H), μ_0 is permeability of free space, μ_T is relative permeability, N is number of turns in wire coil, A the area of coil (m²) and l is the average length of coil (m) [35,36].

Therefore, it can be concluded that increasing the volume fraction of B₄C as reinforcing material, increases the percentage of intermetallic particles.

4. Conclusion

1. At the beginning of immersion of AA5083 aluminium alloy in sodium chloride solution, a passive layer is observed on the surface. However, no passive layer is seen on the composite samples.
2. During extrusion, mechanical alloying and composite operation, shear stresses are applied to intermetallic particles, which cause their crushing and distribution throughout the sample.
3. The composite operation of 5083 aluminium–magnesium alloy reduces its corrosion resistance. Also, increasing the percentage of reinforcing particles results in a further decrease in corrosion resistance of the composite.
4. Increasing the value of B₄C in the composite samples leads to an increase in the content of intermetallic particles as cathodic sites surface area, which enhances cathodic and anodic reactions on the surface.
5. Increasing the value of B₄C in the composite sample, decreases the corrosion resistance of the alloy compared to AA5083 aluminium alloy.

References

- [1] Rammelt U, Koehler S and Reinhard G 2011 *Corros. Sci.* **53** 3515
- [2] Chakrapani P and Suryakumari T S A 2021 *Mater. Today* **45** 5960
- [3] Suthar J and Patel K M 2018 *Mater. Manuf.* **33** 499
- [4] Sharma D K, Sharma M and Upadhyay G 2019 *Int. J. Innov. Technol. Explor. Eng.* **9** 2194
- [5] Hu J, Chu W Y, Fei W D and Zhao L C 2004 *Mater. Sci. Eng. A* **374** 153
- [6] Candan S and Bilgic E 2004 *Mater. Lett.* **58** 2787
- [7] Zhu Y, Sun K and Frankel G S 2018 *J. Electrochem. Soc.* **165** C807
- [8] Birbilis N and Buchheit R G 2005 *J. Electrochem. Soc.* **152** B140
- [9] Aballe A, Bethencourt M, Botana F J, Osuna R and Marcos M 2001 *Werkst. Korros.* **52** 185
- [10] Karabulut H and Karacif K 2023 *GU. J. Sci.* **11** 339
- [11] Abbass M K, Hassan K S and Alwan A S 2015 *IJMMM* **3** 31
- [12] Ahmad Z 2011 (ed.) *Recent trends in processing and degradation of aluminium alloys* (BoD Books on Demand)
- [13] Aziz I and Zhang Q 2009 *Int. J. Mod. Phys.* **23** 1497
- [14] Jafarzadeh K, Shahrabi T and Hosseini M G 2008 *J. Mater. Sci. Technol.* **24** 215
- [15] Alizadeh M and Amini R 2013 *J. Mater. Sci. Technol.* **29** 725
- [16] Yuvaraj N and Sivanandam A 2015 *J. Mater. Res. Technol.* **4** 398
- [17] Singh G and Sharma N 2020 *Mater. Today* **21** 1229
- [18] Alizadeh A, Abdollahi A and Radfar M 2017 *Trans. Non-ferrous Met. Soc. China* **27** 1233
- [19] Alizadeh A, Abdollahi A and Saessi M 2022 *Trans. Indian Inst. Met.* **75** 251
- [20] Saessi M, Alizadeh A and Abdollahi A 2021 *TNMSC* **31** 74
- [21] Jafarzadeh K, Shahrabi T and Oskouei A A 2009 *J. Appl. Electrochem.* **39** 1725
- [22] Sikora E, Wei X J and Shaw B A 2004 *Corrosion* **60** NACE-04040387
- [23] Liu Y, Zhou X, Thompson G E, Hashimoto T, Scamans G M and Afseth A 2006 *J. Phys. Conf. Ser.* **26** 103
- [24] Vasudevan N, Bhaskar G B, Rajendra Prasad A and Suresh S M 2019 *Mater. Today* **16** 1124
- [25] Katkar V A, Gunasekaran G, Rao A G and Koli P M 2011 *Corros. Sci.* **53** 2700
- [26] Brug G J, van den Eeden A L, Sluyters-Rehbach M and Sluyters J H 1984 *J. Electroanal. Chem. Interfacial. Electrochem.* **176** 275
- [27] Hirschorn B, Orazem M E, Tribollet B, Vivier V, Frateur I and Musiani M 2010 *Electrochim. Acta* **55** 6218
- [28] Han Y M and Chen X G 2015 *Mater.* **8** 6455
- [29] Zheng R, Hao X, Yuan Y, Wang Z, Ameyama K and Ma C 2013 *J. Alloys Compd.* **576** 291
- [30] Peltier F and Thierry D 2021 *Corros. Eng. Sci. Technol.* **56** 610
- [31] Mc Cafferty E 2003 *Corros. Sci.* **45** 1421
- [32] Munoz A G and Bessone J B 1999 *Corros. Sci.* **41** 1447
- [33] Szklarska-Smialowska Z 1999 *Corros. Sci.* **41** 1743
- [34] Blanc C and Mankowski G 1997 *Corros. Sci.* **39** 949
- [35] Inductance. Available: www.electronics-tutorials.com (22nd May 2002)
- [36] Inductors. Available: www.hyperphysics.phy-astr.gsu.edu 2006

Springer Nature or its licensor (e.g. a society or other partner) holds exclusive rights to this article under a publishing agreement with the author(s) or other rightsholder(s); author self-archiving of the accepted manuscript version of this article is solely governed by the terms of such publishing agreement and applicable law.